JOURNAL OF MATERIALS SCIENCE 29 (1994) 4866–4874

Evolution of the microstructure of undoped and Nb-doped $SrTiO_3$

S. G. CHO
Department of Electronic Materials Engineering, Gyeongsang National University, Chinju, Gyeongnam 660-701, Korea

P. F. JOHNSON
NYS College of Ceramics, Alfred University, Alfred, NY 14802, USA

Undoped and Nb-doped $SrTiO_3$ specimens with excess titania compositions were prepared by sintering in air at 1420 or 1480 °C. Large grains due to liquid-phase sintering were obtained for undoped specimens containing $\geqslant 0.6$ mol% excess titania and fired at 1480 °C. On the other hand uniform fine grains were observed for samples fired at 1420 °C, resulting from grain-growth inhibition due to exsolved TiO_2 second phase. The solubility of excess titania seemed less than 0.2 mol% under our experimental conditions. The microstructural behaviour of Nb-doped $SrTiO_3$ could be explained well by the Sr-vacancy compensation model. According to this model, the solubility of excess titania in $SrTiO_3$ increased with Nb_2O_5 dopant concentration. Thus, for specimens which had high excess titania compositions and were sintered at 1480 °C, large grains were observed when the Nb content was low enough to retain sufficient excess titania-forming liquid phase. For specimens having the same compositions and fired at 1420 °C, uniform fine grains were obtained due to grain growth inhibition by the exsolved TiO_2 second phase, when the Nb content was low. If the excess titania was less than the solubility determined by the amount of Nb dopant, Ruddlesden–Popper-type phases were believed to be formed and resulted in poor densification. Although excess titania was the major factor in determining the grain size of the specimens, the niobium dopant enhanced grain growth.

1. Introduction

Strontium titanate ($SrTiO_3$) is one of the perovskite-structure materials which have been widely used in the electronic ceramic industry. Specifically, $SrTiO_3$ is used for internal boundary layer (IBL) capacitors because of its high dielectric constant and excellent stability with temperature and applied voltage [1–3]. Its application has been expanded to electrodes for the photoassisted electrolysis of water [4, 5] and the oxygen sensors [6].

As expected from the crystal structure and the elements comprising the material, $SrTiO_3$ exhibits characteristics similar to $BaTiO_3$. Studies have shown the defect chemistry of undoped or doped $SrTiO_3$ to be nearly identical to that of $BaTiO_3$ [7–10]. Like $BaTiO_3$ ceramics, donor-type dopants are often added in order to obtain useful electrical properties. Although the defect structures and incorporation of donor elements in $SrTiO_3$ are expected to be very similar to those of donor-doped $BaTiO_3$, the electrical properties at room temperature are quite different. It is well known that donor-doped $BaTiO_3$ sintered in air exhibits a conductivity anomaly and a grain-size anomaly with respect to donor concentration [11–13]. However, this behaviour has not been reported for donor-doped $SrTiO_3$.

The microstructure of $BaTiO_3$ ceramics has been extensively studied [14–17], whereas only a few studies may be found for $SrTiO_3$ [8, 18–20]. The microstructures of $SrTiO_3$-based IBL capacitors, which consist of donor-doped semiconducting grains and mixed-oxide insulating grain boundary phases, have been investigated. The investigations focused primarily on the grain boundary phases [2, 21]. Since SiO_2 and Al_2O_3 or GeO_2 are usually added to control the microstructure of the $SrTiO_3$ conductive grains, the effect of donor dopants, such as niobium, on the microstructure of $SrTiO_3$ ceramics is hard to identify in these IBL capacitors.

In the present study, the microstructure of undoped and Nb-doped $SrTiO_3$ sintered in air was investigated as a function of excess titania and/or niobium dopant concentration. Since defect structure, type of defects and defect concentration play an important role in $SrTiO_3$, the microstructural behaviour was interpreted in terms of defect chemistry.

2. Experimental procedure

Strontium titanate powder was prepared using the Pechini process [22]. First, a Ti-organic solution batch was prepared and the appropriate amount of

0022–2461

reagent-grade $SrCO_3$ (Baker Chemical, Philipsburg, New Jersey), powder was dissolved into a small amount of this solution to produce the desired compositions. To obtain Nb-doped $SrTiO_3$, quantitative addition of a niobium oxalate solution (Cabot Corp., Boyertown, Pennsylvania) was made to the solution. After the solution cleared, heat was applied to form a resin which was then calcined at 900 °C for 3 h in flowing air to form $SrTiO_3$. Since the calcined product was not a fine powder but rather coarse, brittle agglomerates, the agglomerates were ground using an agate mortar and pestle. The ground powder was humidified to improve pressability. No binders were used. Details of the powder preparation are given elsewhere [23].

Disc-shape green pellets were dry-pressed at 140 MPa using a carbon steel die set. The samples were 1.27 cm in diameter and 1.5–2.0 mm thick. Pressed pellets were placed on an alumina setter covered with a platinum sheet and sintered in a furnace under the ambient atmosphere. Two different sintering conditions, 1420 °C for 8 h and 1480 °C for 4 h, were employed at a heating rate of 1.7 °C min^{-1} and a fast cooling rate.

The compositions used in this study were $SrTiO_3 + yTiO_2$ ($0.000 \leqslant y \leqslant 0.014$) for undoped $SrTiO_3$, and Sr/(Ti + Nb) = 0.996 and 0.986 with 0.1–1.5 mol % Nb_2O_5 for donor-doped $SrTiO_3$. The composition of stoichiometric undoped $SrTiO_3$ was repeatedly determined using wet chemical analysis. Semi-quantitative spectrographic analysis of the calcined powder showed that major impurities were Si and Ca. Since SiO_2 affects microstructure significantly, the content was further examined using induction-coupled plasma atomic absorption spectroscopy (ICP-AAS). The amount of SiO_2 present in the final powder was $\leqslant 0.02$ wt %. The Nb dopant concentration was also determined using ICP-AAS, and agreed very well with the amount added. The results of ICP-AAS analysis were obtained from a commercial analytical laboratory (Corning Engineering Laboratory Services, Corning, New York).

For microstructure analysis, sintered specimens were cut using a low-speed diamond saw and polished to 0.3 μm alumina finish. The polished surface was etched with a mixture of HNO_3 and HF solution, and examined using a scanning electron microscope (Autoscan from Etec Corp., Hayward, California) equipped with an energy-dispersive spectrometer (Princeton Gamma-Tech, Princeton, New Jersey). Average grain size was determined by measuring the mean linear intercept of the grains as described by Underwood [24] and Mendelson [25]. Several specimens were prepared for transmission electron microscopy (2000FX from Jeol, Tokyo) and energy-dispersive spectroscopy (EDS) analysis by polishing and subsequent ion-milling. The bulk density of the sintered specimen was measured according to the ASTM standard [26].

The phase identification of the calcined powder and lattice parameter measurements for the sintered samples were carried out using X-ray diffractometers (Norelco from Philips Electronic Inst., Mount Vernon, NY; Kristalloflex 810 from Siemens, Germany). For the lattice parameter measurements, sintered pellets were ground using an agate mortar and pestle, and mixed with silicon powder as an internal standard. X-ray diffraction patterns were collected at $10° \leqslant 2\theta \leqslant 90°$ using CuK_α radiation, and analysed using the National Institute of Standard and Technology's least-squares fitting program.

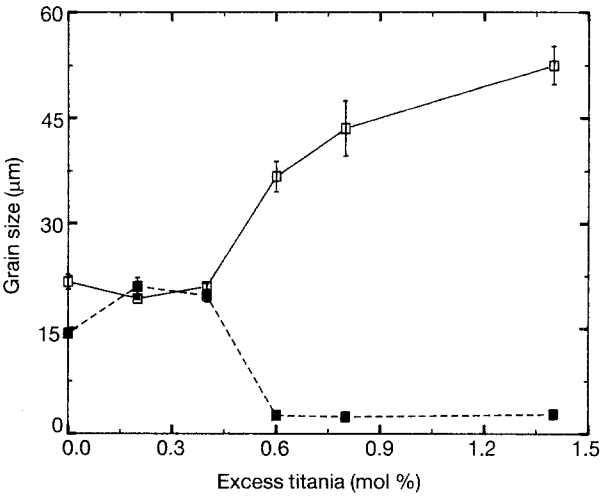

Figure 1 Effect of excess titania on the average grain size of undoped $SrTiO_3$ specimens sintered at different temperatures in air: (□) 1480 °C for 4 h, (■) 1420 °C for 8 h. The specimens containing 0.2 and 0.4 mol % excess titania and fired at 1420 °C have small grains (~ 5 μm) which were not counted in the average grain size measurement.

3. Results and discussion

First the microstructures of undoped samples were examined. Fig. 1 shows the average grain size of the sintered specimens as a function of excess titania content. The samples containing 0.2 and 0.4 mol % excess titania and sintered below the eutectic temperature at 1420 °C consisted of 30–40% fine grains (4–5 μm), and the average grain size shown in Fig. 1 does not reflect these grains due to difficulty in measurement. The effect of excess titania becomes very clear when its content reaches 0.6 mol %. However, the effect was developed in two different ways depending on the sintering temperature. The samples sintered at 1420 °C showed grain-growth inhibition, and those sintered at 1480 °C (above the eutectic temperature) showed grain-growth enhancement.

Typical microstructures of the sintered samples are shown in Fig. 2. The samples in Fig. 2 contained excess titania. An exsolved second phase (generally brighter than $SrTiO_3$ grains) is observed in all samples. The second phase was mainly found in triple grain junctions, but those found in the fine-grain samples were usually particle-like and large in number, whereas in the large-grain samples they were large in size but small in number.

The microstructure of these samples can be easily understood on the basis of their eutectic temperature. Since the eutectic temperature in the binary $SrTiO_3$–TiO_2 system is 1440 °C [27], a liquid phase

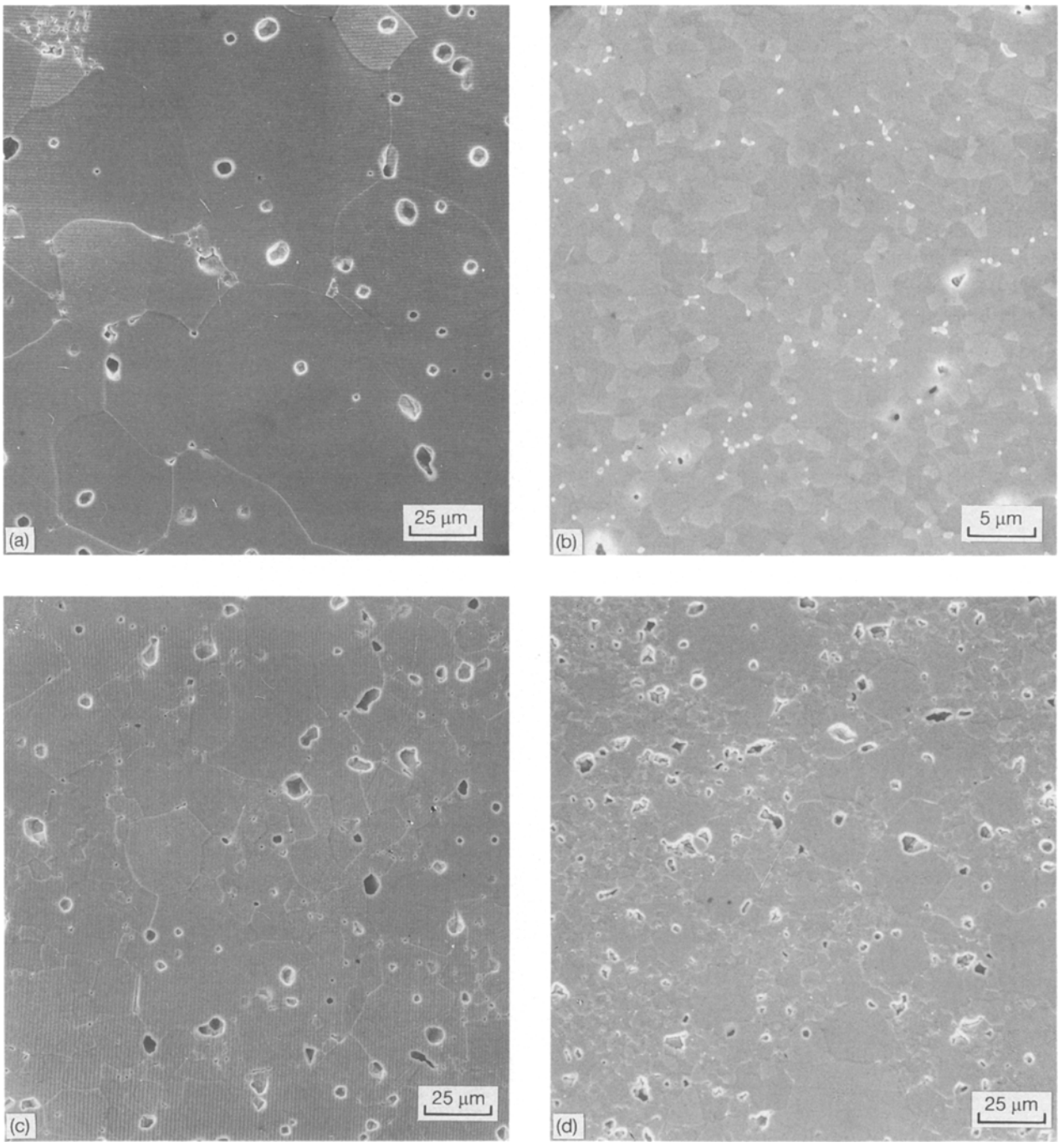

Figure 2 Scanning electron micrographs of undoped $SrTiO_3$ specimens sintered in air: (a) Sr/Ti = 0.986, 1480 °C for 4 h; (b) Sr/Ti = 0.986, 1420 °C for 8 h; (c) Sr/Ti = 0.996, 1480 °C for 4 h; (d) Sr/Ti = 0.996, 1420 °C for 8 h.

formed in all samples sintered at 1480 °C which surrounded the grains and enhanced the grain growth when the amount of liquid phase was sufficient (high excess titania), whereas the samples sintered at 1420 °C had a discrete solid second phase formed during sintering. The amount of the second phase was determined by the solubility of excess titania in the $SrTiO_3$ lattice, and when the amount of second phase in the grain boundaries was large, grain-growth inhibition occurred.

EDS analysis of the second phase exhibited very strong titanium peaks and weak strontium peaks. This result agrees with the observation of Witek *et al.* [8] and the second phase is believed to be TiO_2. Experimental proof of the composition of this phase will be discussed further for the case of Nb-doped samples, where EDS analysis was carried out in the TEM mode. Bulk densities of these samples were about 97% of theoretical density, and no significant differences were observed either with respect to the sintering temperature or excess titania content. The colours of the sintered specimens were all yellowish brown.

The solubility of excess titania is important to both the defect chemistry and microstructure development of $SrTiO_3$. Witek *et al.* [8] suggested that the solubility of excess titania in $SrTiO_3$ is less than 0.5 mol %, whilst Eror and Balachandran [9] reported that no second phase was detected up to 2 mol % excess

titania. The present results based on the micrographs of polished and etched surfaces show the solubility of excess titania to be less than 0.2 mol %.

Microstructures of the sintered samples investigated in the present study can be classified into three groups, based on grain size: fine grains (3–5 μm), normal grains (14–22 μm) and large grains (35–100 μm). For convenience, the microstructure will be described using these three expressions for the grain size.

The microstructures of Nb-doped samples were also examined. The composition of samples having a fixed A-site to B-site ratio of 0.996 can be expressed as $SrTi_{1-x}Nb_xO_3 + 0.004TiO_2$ ($0.002 \leqslant x \leqslant 0.020$). Average grain sizes of the specimens sintered at 1480 °C are shown in Fig. 3. The large grain size of the specimens containing 0.4 at % Nb was an unexpected result. As was determined for the undoped samples containing excess titania, enhanced grain growth was observed for excess titania $\geqslant 0.6$ mol %. Since these doped samples contained only 0.4 mol % excess titania, enhanced grain growth due to excess titania was not expected. Indeed, the samples containing 0.2 and 0.8 at % Nb show normal grain sizes; however, a large grain size was observed for 0.4 at % Nb and very fine grain sizes for $\geqslant 1.2$ at % Nb. Quantitative measurement of those very fine grains was not possible, because the samples were very porous. The specimens sintered at 1420 °C exhibited a similar trend but some fine grains were present. The specimens containing 1.0 at % Nb and sintered at 1420 °C had very fine grains and porous structures, whilst those sintered at 1480 °C had small grains and dense structure. All of the specimens containing $\geqslant 1.2$ at % Nb showed poor densification regardless of sintering temperature. This is shown in Fig. 4, which plots the densities of the samples as a function of Nb concentration. These results will be interpreted later in conjunction with the results of samples having A/B = 0.986.

Assuming that all donor-dopants are incorporated into the lattice, the compositions of the second set of Nb-doped samples investigated can be expressed as $SrTi_{1-x}Nb_xO_3 + 0.014TiO_2$ ($0.002 \leqslant x \leqslant 0.030$). Average grain sizes of the sintered specimens of this composition are shown in Fig. 5. The samples containing Nb up to 1.4 at % exhibited an enhanced grain growth when fired above the liquid phase formation temperature, and a grain-growth inhibition when sintered below the liquid phase formation temperature. The microstructural evolution of these samples was similar to that of the undoped specimens which contained $\geqslant 0.6$ mol % excess titania. However, the specimens containing 2.2 at % Nb had normal grains.

A batch of powder containing 1.6 at % Nb was prepared as Sr/(Ti + Nb) = 0.988, or 1.2 mol % excess titania, instead of 0.986. The average grain size of these specimens, sintered at 1480 °C, was 21.5 ± 1.2 μm, whilst the specimens sintered at 1420 °C consisted of large grains (~ 40 μm) and fine grains (~ 5 μm). The specimens containing 3.0 at % Nb were poorly sintered at both sintering temperatures. Typical microstructures of the Nb-doped samples are shown in Fig. 6. The specimens were about 97% of theoretical density except the specimens containing 3.0 at % Nb, which were less than 85%.

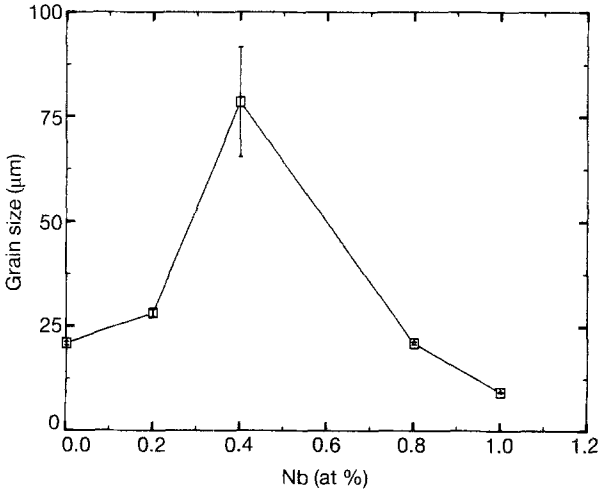

Figure 3 Average grain size as a function of Nb concentration for samples having Sr/(Ti + Nb) = 0.996 and sintered at 1480 °C.

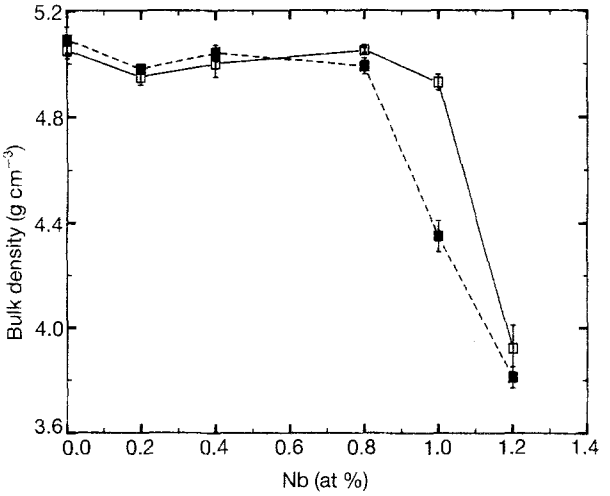

Figure 4 Bulk density as a function of Nb concentration for samples having Sr/(Ti + Nb) = 0.996 and sintered in air: (□) 1480 °C for 4 h, (■) 1420 °C for 8 h.

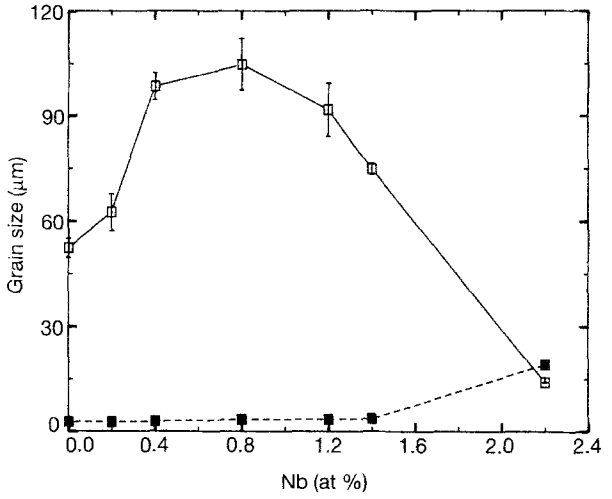

Figure 5 Average grain size as a function of Nb concentration for samples having Sr/(Ti + Nb) = 0.986 and sintered in air: (□) 1480 °C for 4 h, (■) 1420 °C for 8 h.

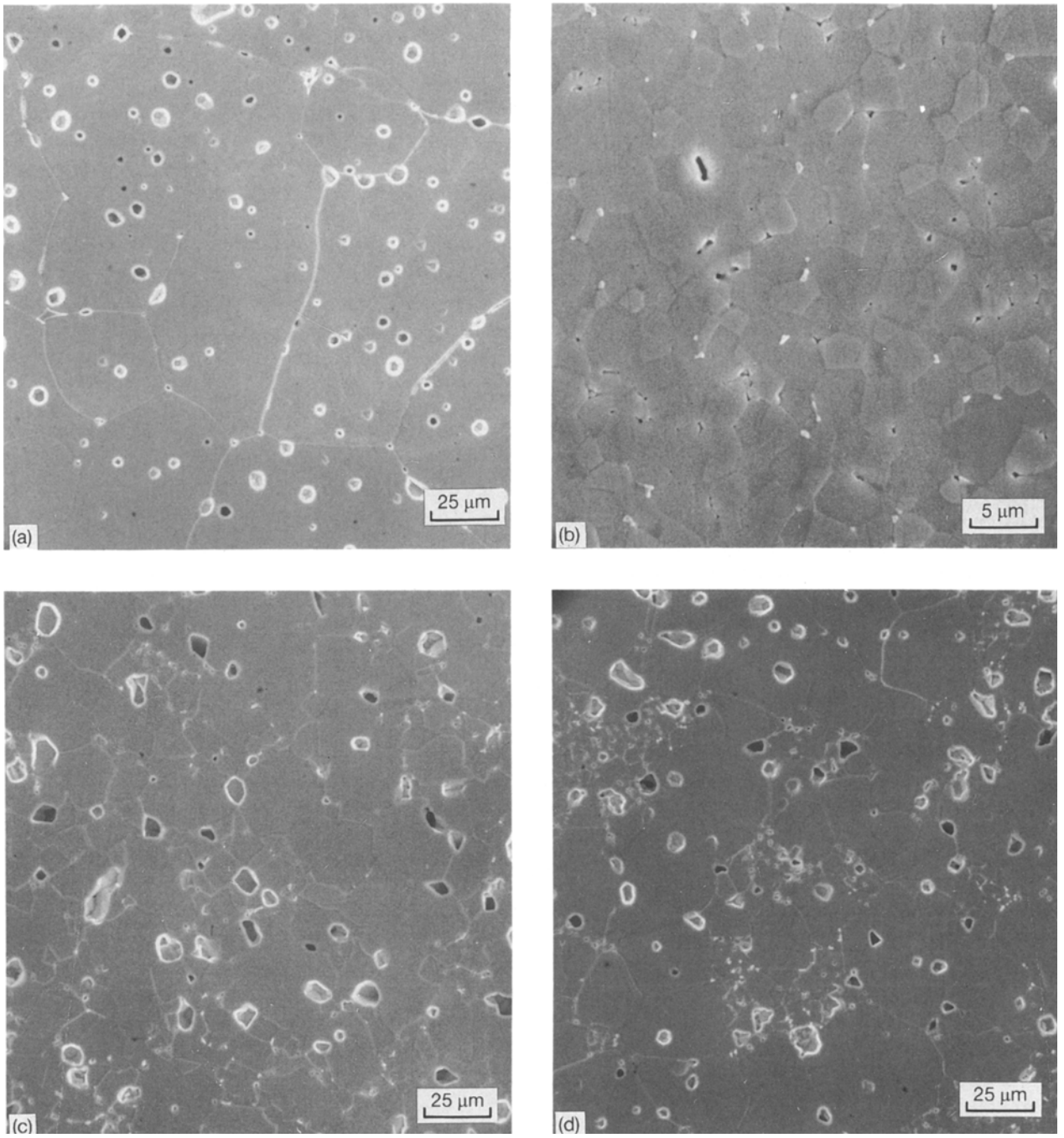

Figure 6 Scanning electron micrographs of specimens containing various Nb concentrations (Sr/(Ti + Nb) = 0.986): (a) 1.2 at % Nb, sintered at 1480 °C for 4 h; (b) 1.2 at % Nb, sintered at 1420 °C for 8 h; (c) 2.2 at % Nb, sintered at 1480 °C for 4 h; (d) 2.2 at % Nb, sintered at 1420 °C for 8 h.

The porosity, especially intergranular pores found in large grains, can be understood from the characteristics of the starting powder. Fig. 7 shows a transmission electron micrograph of the calcined powder. The particles are very fine (a few hundred nanometres) but form strong agglomerates.

The microstructural behaviour of Nb-doped specimens was initially difficult to interpret. If all the niobium ions were incorporated in the lattice following the electronic compensation mechanism, i.e. $Sr^{2+}Nb_x^{5+}Ti_x^{3+}Ti_{1-x}^{4+}O_3^{2-}$, all samples would have 1.4 mol % excess titania. First, the samples sintered at 1480 °C were considered. Assuming sintering and grain growth to be governed by the amount of liquid phase present during sintering, the sintered microstructures should be similar to those for the undoped samples sintered at the same temperature. Since the solubility of excess titania in $SrTiO_3$ is very limited as determined from the microstructures of the undoped samples previously investigated and the phase diagram [27], the amount of liquid phase is determined by the amount of excess titania added. Grain growth should then be observed for these specimens, but this does not agree with the experimental result.

Secondly, the samples sintered at 1420 °C were considered. As was observed for undoped and TiO_2-excess samples, grain-growth inhibition occurred when excess TiO_2 content reached 0.6 mol %. Since

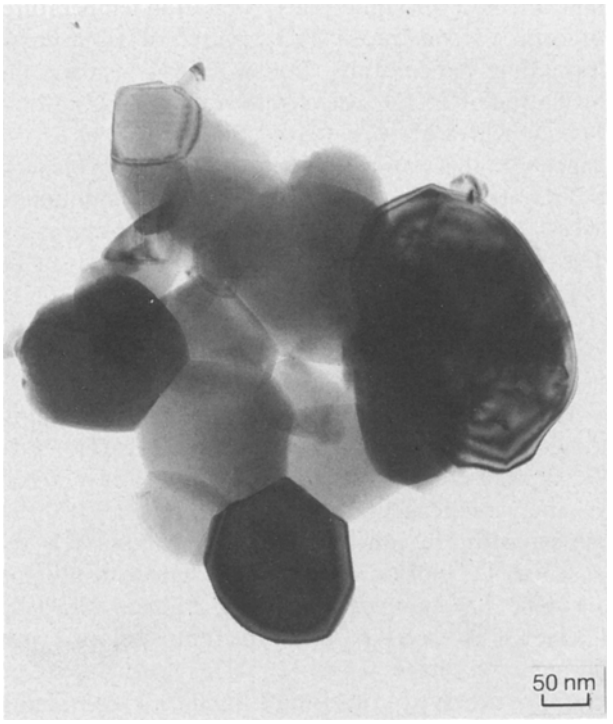

Figure 7 Transmission electron micrograph of the calcined powder which is stoichiometric undoped $SrTiO_3$ dispersed in alcohol.

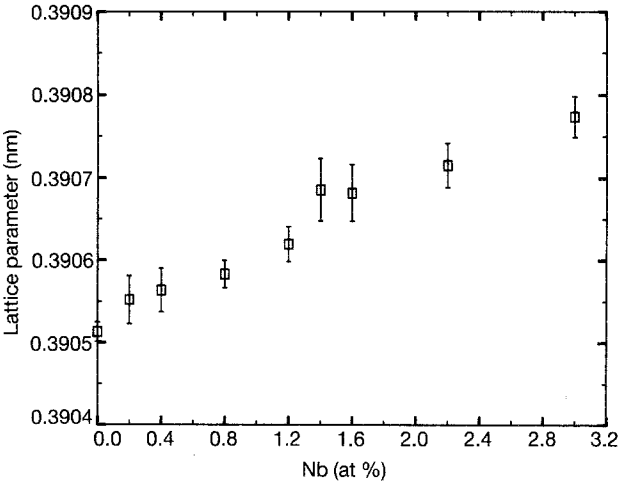

Figure 8 Lattice parameters determined by X-ray diffraction for samples having Sr/(Ti + Nb) = 0.986 and sintered at 1480 °C for 4 h.

Figure 9 Transmission electron micrograph of a sample containing 1.4 at % Nb and sintered at 1420 °C for 8 h (Sr/(Ti + Nb) = 0.986). Dark spots are where EDS analysis were carried out. A TiO_2 second phase is observed in the upper right-hand side.

the amount of excess TiO_2 in these Nb-doped samples is greater than 0.6 mol %, grain-growth inhibition should prevail in all samples. However, this does not agree with the experimental result either. In order to understand the microstructural behaviour of Nb-doped samples, several situations were considered and examined, including (i) a solubility limit or segregation of Nb, (ii) sintering totally controlled by Nb, and (iii) solubility of excess titania increasing with Nb concentration.

The solubility limit of Nb was investigated by lattice parameter measurements using X-ray diffraction. Fig. 8 shows lattice parameters determined as a function of Nb concentration. The lattice parameter increased with Nb concentration up to 3.0 at %, suggesting that the solubility limit of Nb was not reached within the compositions studied. Also, incorporation of Nb in $SrTiO_3$ up to 2.5 at % has been reported for air-fired samples [18].

Compositional variation was investigated using an analytical scanning transmission electron microscope. EDS analysis was performed on the grain boundary and several regions gradually further from the grain boundary as indicated in Fig. 9. The results indicated no compositional variation for either the Sr to Ti ratio or the Nb content, within the detection limit. EDS analysis for the second phases in the samples, sintered either at high temperature or low temperature, showed strong Ti peaks and traces of Sr and Nb, presumably from the matrix phase activated by the finite beam spread in the sample. Electron diffraction patterns of the second phase confirmed that these are crystalline phases. It is believed that the second phase is TiO_2 as was reported by Witek *et al.* [8] and Stenton and Harmer [20].

The hypothesis that sintering is totally controlled by Nb dopant is not convincing. Although the grain size and densification of Nb-doped specimens were both affected by Nb concentration, the Nb concentration causing these affects was very different for samples having Sr/(Ti + Nb) = 0.996 and 0.986. It can therefore be concluded that Nb concentration is responsible for the microstructural behaviour, but only indirectly.

The increase of solubility of excess titania in $SrTiO_3$ with Nb concentration was investigated carefully. Chan *et al.* [7] suggested that the solubility of excess titania may be enhanced by the tendency of the Nb_2O_5 content to reduce the $V_O^{\cdot\cdot}$ content. Considering only accommodation of excess titania and Nb_2O_5 in the lattice:

$$TiO_2 \rightarrow Ti_{Ti} + 2O_O + V''_{Sr} + V_O^{\cdot\cdot}$$

$$Nb_2O_5(-2TiO_2) \rightarrow 2Nb_{Ti} + 4O_O + \frac{1}{2}O_2 + 2e'$$

The solubility increase of excess TiO_2 is proportional to the niobia concentration, and the summation of the above two equations results in Sr vacancy compensation for donor centres. Thus, maximum solubility of excess TiO_2 can be achieved when Nb donor centres are compensated by Sr vacancies.

Since it became clear that defect structure plays an important role in the microstructural evolution of donor-doped $SrTiO_3$, defect models for Nb-doped $SrTiO_3$ were examined. For stoichiometric compositions, i.e. Sr/(Ti + Nb) = 1.000, assuming electronic compensation, the reaction of the starting composition can be expressed as

$$SrO + (1 - x)TiO_2 + \frac{x}{2}Nb_2O_5 \rightarrow SrNb_x^{\cdot}Ti_x'Ti_{1-2x}O_3 + \frac{x}{4}O_2 \quad (1)$$

Assuming vacancy compensation (only the Sr vacancy was considered because the Ti vacancy was structurally unfavourable), one may write

$$SrO + (1 - x)TiO_2 + \frac{x}{2}Nb_2O_5 \rightarrow Sr_{1-(x/2)}(V_{Sr}'')_{x/2}Nb_x^{\cdot}Ti_{1-x}O_3 + \frac{x}{2}SrO \quad (2)$$

If the samples have excess TiO_2, i.e. Sr/(Ti + Nb) = $1/(1 + y)$, and assuming electronic compensation, the equation can be expressed as

$$SrO + (1 - x + y)TiO_2 + \frac{x}{2}Nb_2O_5 \rightarrow SrNb_x^{\cdot}Ti_x'Ti_{1-2x}O_3 + yTiO_2 + \frac{x}{4}O_2 \quad (3)$$

and assuming vacancy compensation

$$SrO + (1 - x + y)TiO_2 + \frac{x}{2}Nb_2O_5 \rightarrow Sr_{1-(x/2)}(V_{Sr}'')_{x/2}Nb_xTi_{1-x}O_3 + \frac{x}{2}SrTiO_3 + \left(y - \frac{x}{2}\right)TiO_2 \quad (4)$$

Equation 1 is the most common description for electronic compensation of donor-doped $SrTiO_3$ or $BaTiO_3$. Here, niobium donors are compensated by the creation of Ti^{3+} ions. Equation 2 is almost the same as the equation for stoichiometric La-doped $SrTiO_3$ suggested by Balachandran and Eror [28]. The SrO in the right-hand side of Equation 2 is thought to be present as a structural accommodation in the perovskite structure like a Ruddelsden–Popper type of phase [29]. For stoichiometric La-doped $SrTiO_3$, the formation of a Ruddelsden–Popper phase at high oxygen partial pressure has been suggested [10, 28]. Defect energy calculations using atomistic computer simulation techniques support the presence of this phase for SrO-rich $SrTiO_3$ [30]. Equation 3 is same as Equation 1 except for the exsolution of excess TiO_2 in the grain boundary area. The exsolved excess TiO_2 forms a liquid phase by reaction with the $SrTiO_3$ matrix above the liquid-phase formation temperature, or forms a second phase (TiO_2) below the liquid-phase formation temperature. Equation 4 considers the formation of $SrTiO_3$ between the excess TiO_2 and the Sr ions which are released by the creation of Sr vacancies. In this way the solubility of excess TiO_2 in the $SrTiO_3$ lattices increases, and hence the amount of excess TiO_2 present in the grain boundaries decreases. The structure determined using Equation 4 can be rewritten as

$$Sr(V_{Sr}'')_{x/2}Nb_x^{\cdot}Ti_{1-(x/2)}O_{3[1+(x/2)]} + \left(y - \frac{x}{2}\right)TiO_2.$$

Table I shows the amount of excess TiO_2 present in the grain boundaries for samples having Sr/(Ti + Nb) = 0.986, in accordance with Equations 3 and 4. When vacancy compensation is employed, excess TiO_2 decreases with Nb concentration. The excess TiO_2 reduces to 0.7 mol % when the Nb concentration is 1.4 at %. The samples containing 2.2 at % Nb have 0.3 mol % excess TiO_2, whilst the samples doped with 1.6 at % Nb have 0.4 mol %. Therefore, the large grains observed in the samples containing 0.2–1.4 at % Nb and sintered at 1480 °C can be explained by liquid-phase sintering in which the amount of liquid phase is determined by the amount of excess TiO_2 present in the grain boundaries. Also the other microstructural behaviour can be completely understood in the same manner.

The amount of excess TiO_2 present in the grain boundaries for samples having Sr/(Ti + Nb) = 0.996

TABLE I Excess TiO_2 present in the grain boundaries for different compensation mechanisms (Sr/(Ti + Nb) = 0.986)

Nb (at %)	Excess TiO_2 (mol %)	
	Electronic[a]	Vacancy[b]
0.2	1.4	1.3
0.4	1.4	1.2
0.8	1.4	1.0
1.2	1.4	0.8
1.4	1.4	0.7
1.6	1.2[c]	0.4
2.2	1.4	0.3
3.0	1.4	0.1

[a] $100y$: refer Equation 3.
[b] $100(y - x/2)$: refer Equation 4.
[c] This composition has A/B = 0.988.

TABLE II Excess TiO_2 present in the grain boundaries for different compensation mechanisms (Sr/Ti + Nb) = 0.996)

Nb (at %)	Excess TiO_2 (mol %)	
	Electronic[a]	Vacancy[b]
0.2	0.4	0.3
0.4	0.4	0.2
0.8	0.4	0.0
1.0	0.4	− 0.1
1.2	0.4	− 0.2
2.0	0.4	− 0.6

[a] $100y$: refer Equation 3.
[b] $100(y - x/2)$: refer Equation 4.

is shown in Table II. Again, the normal grains observed in the samples containing 0.2 and 0.8 at % Nb can be understood in terms of the amount of excess TiO_2 in the grain boundaries. Notable are negative values of excess TiO_2 found for samples containing $\geqslant$ 1.0 at % Nb. A negative value is also found for samples having Sr/(Ti + Nb) = 0.986 and 3.0 at % Nb, as shown in Table I. The meaning of a negative value of excess TiO_2 is that those samples do not have sufficient excess titania to form $SrTiO_3$ with the Sr ions exsolved from the lattice through the compensation of donor centres by Sr vacancies. Thus, the Sr ions which do not form $SrTiO_3$ may form SrO layers and be accommodated in the structure as Ruddelsden–Popper layers. This can be a reason why those samples could not be sintered well under the present sintering conditions. One may expect that the densification of specimens having a complicated ordered structure such as the Ruddelsden–Popper phase is very difficult to achieve. It has often been observed that SrO-rich $SrTiO_3$ samples are porous and low in density [13, 19].

The average grain sizes of the undoped samples and Nb-doped samples sintered at 1480 °C as a function of excess titania are given in Fig. 10. The same plot for the samples sintered at 1420 °C is given as Fig. 11. Here, excess titania content for Nb-doped samples was determined by Equation 4. The change of grain size with excess titania for both undoped and Nb-doped samples shows the same trend. The net effect of Nb can be deduced from differences between the curves of undoped and Nb-doped samples. Niobium does enhance the grain growth of the samples containing a sufficient amount of excess titania, presumably due to the increase of Sr vacancy concentration caused by the accommodation of Nb ions. Apparently diffusion of Sr ions is enhanced by the increased Sr vacancy concentration, since vacancy diffusion is the most probable diffusion mechanism for perovskite-structure material [31].

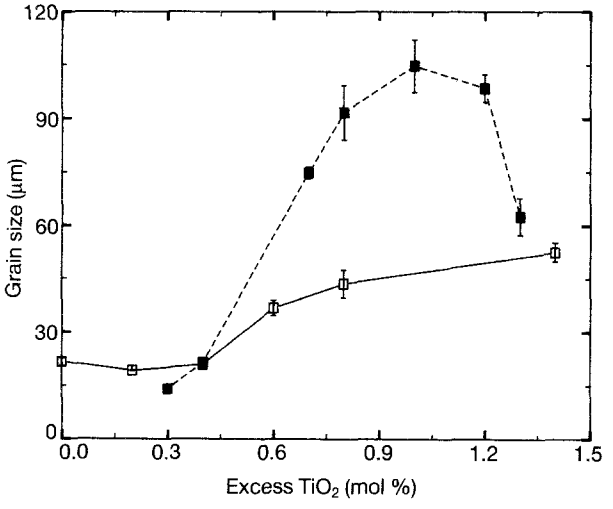

Figure 10 Average grain size as a function of excess TiO_2 present in the grain boundary region for samples sintered at 1480 °C for 4 h: (□) undoped samples, (■) Nb-doped samples having Sr/(Ti + Nb) = 0.986. Excess TiO_2 for Nb-doped samples were determined using Equation 4 (see also Table I).

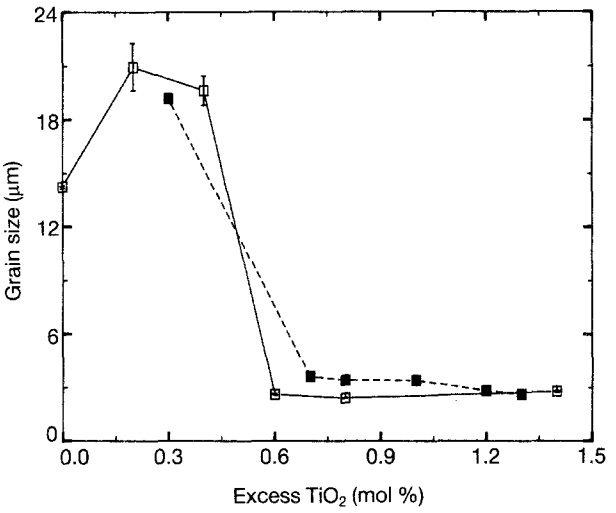

Figure 11 Average grain size as a function of excess TiO_2 present in the grain boundary region for samples sintered at 1420 °C: (□) undoped samples, (■) Nb-doped samples having Sr/(Ti + Nb) = 0.986.

In order to check the validity of our interpretation for Nb-doped $SrTiO_3$ sintered in air, samples having an A/B = 0.988 and doped with 1.6 at % Nb and those having A/B = 0.986 and doped with 2.2 at % Nb were sintered at 1480 °C for 4 h in a 90% N_2–10% H_2 gas flow. These samples showed large grains, in contrast to the air-fired samples which showed normal grains. Because donor-doped $SrTiO_3$ is electronically compensated when sintered under a reducing atmosphere [28], these samples have sufficient excess TiO_2 to form a liquid phase during sintering in accordance with Equation 3, resulting in large grains.

The abrupt decrease of grain size by a very small increase in donor concentration (0.05 at %) found in donor-doped $BaTiO_3$ ceramics [13, 17] was not observed in the present experiment. Moreover the colour of the specimens, which indicates the conductive or insulating nature of the grains, does not coincide with the grain size. Samples containing $\leqslant$ 0.4 at % Nb had a brownish colour, whilst the samples containing $\geqslant$ 0.8 at % Nb showed a dark greyish colour, regardless of grain sizes. The electrical properties of Nb-doped specimens were reported elsewhere [32]. However, the effect of excess titania and Nb concentration on the grain size observed in the Nb-doped $BaTiO_3$ ceramics containing $\geqslant$ 0.35 at % Nb, and sintered at high temperature in air, agrees with the present results [17].

Although it is clear that niobium content enhances grain growth, the large grains observed in the samples having an A/B = 0.996 and 0.4 at % Nb as shown in Fig. 3 are not yet understood. Again, since these samples exhibited a brownish colour, the grain-size anomaly observed in $BaTiO_3$ cannot be considered. Such a large grain size was also observed in an air-fired $SrTiO_3$ which contains 0.2 at % Y but does not have appreciable excess titania [18]. Since the authors could not prepare another batch for this particular composition, the possibility of experimental error cannot be excluded.

4. Conclusions

Air-fired, TiO_2-rich $SrTiO_3$ ceramics showed large grains when the samples contained excess $TiO_2 \geqslant 0.6$ mol % and were sintered at temperatures higher than the liquid-phase formation temperature. The grain size increased with the excess TiO_2 content. In contrast, fine grains were obtained when the same samples were sintered below the liquid-phase formation temperature. Grain-growth inhibition observed for samples fired at low temperature was attributed to the TiO_2 second phase exsolved at the grain boundaries.

Titania second phase was clearly distinguished from the matrix $SrTiO_3$ grains in electron micrographs by chemical etching. The solubility of excess TiO_2 in $SrTiO_3$, determined by scanning electron microscopy, was less than 0.2 mol % under our experimental conditions.

The microstructural behaviour of Nb-doped $SrTiO_3$ ceramics sintered in air could be explained using an Sr vacancy compensation model. According to this model, the solubility of excess TiO_2 increased with the Nb_2O_5 dopant concentration, and hence the loss of excess TiO_2 due to high dopant concentration can be understood. Also, the poor densification observed in some Nb-doped samples could be explained using this model in conjunction with the formation of a Ruddelsden–Popper type of phase. Although the amount of excess TiO_2 governs the sintering of these materials, niobium did enhance grain growth, presumably by increasing the diffusion rate of strontium ions.

The solubility of Nb in $SrTiO_3$ seems higher than 3.0 at % under our experimental conditions. The lattice parameter of Nb-doped $SrTiO_3$ determined using an X-ray diffractometer showed a constant increase with Nb concentration up to 3.0 at %.

References

1. G. GOODMAN, in "Advances in Ceramics", Vol. 1, edited by L. M. Levinson and D. C. Hill (American Ceramic Society, Westerville, Ohio, 1981) p. 215.
2. N. YAMAOKA and T. MATSUI, *ibid.* p. 232.
3. H. D. PARK and D. A. PAYNE, *ibid.* p. 242.
4. V. W. R. AMARAKOON, PhD thesis, University of Illinois-Urbana Champaign (1980).
5. M. S. WRIGHTON, A. B. ELLIS, P. T. WOLCZANSKI, D. L. MORSE, H. B. ABRAHAMSON and D. S. GINLEY, *J. Amer. Chem. Soc.* **98** (1976) 2774.
6. T. SEIYAMA, H. ARAI, H. NIITA and K. YASUGATA, Japanese Patent 60 225 051 (1985).
7. N. H. CHAN, R. K. SHARMA and D. M. SMYTH, *J. Electrochem. Soc.* **128** (1981) 1762.
8. S. WITEK, D. M. SMYTH and H. PICKUP, *J. Amer. Ceram. Soc.* **67** (1984) 372.
9. N. G. EROR and U. BALACHANDRAN, *J. Solid State Chem.* **42** (1982) 227.
10. *Idem, ibid.* **40** (1981) 85.
11. G. H. JONKER, *Solid State Electronics* **7** (1964) 895.
12. W. HEYWANG, *J. Mater. Sci.* **6** (1971) 1214.
13. R. WERNICKE, *Phys. Status Solidi (a)* **47** (1978) 139.
14. M. KAHN, *J. Amer. Ceram. Soc.* **54** (1971) 452.
15. T. MURAKAMI, T. MIYASHITA, M. NAKAHARA and E. SEKINE, *ibid.* **56** (1973) 294.
16. M. DROFENIK, A. POPOVIC and D. KOLAR, *Amer. Ceram. Soc. Bull.* **63** (1984) 702.
17. K. LUBITZ, in "Sintering – Theory and Practice", Proceedings of 5th International Round Table Conference on Sintering, Portorž, Yugoslavia, 7–10 September 1981, p. 343.
18. I. BURN and S. NEIRMAN, *J. Mater. Sci.* **17** (1982) 3510.
19. M. RAYMOND, MS thesis, Alfred University (1987).
20. N. STENTON and M. P. Harmer, in "Advances in Ceramics", Vol. 7, edited by M. F. Yan and A. H. Heuer (American Ceramic Society, Westerville, Ohio, 1983) p. 156.
21. R. WERNICKE, in "Advances in Ceramics", Vol. 1, edited by L. M. Levinson and D. C. Hill (American Ceramic Society, Westerville, Ohio, 1981) p. 261.
22. M. P. PECHINI, US Patent 3 330 697 (1967).
23. S. G. CHO, P. F. JOHNSON and R. A. CONDRATE Sr, *J. Mater. Sci.* **25** (1990) 4738.
24. E. UNDERWOOD, "Quantitative Stereology" (Addison-Wesley, New York, 1970) p. 23.
25. M. I. MENDELSON, *J. Amer. Ceram. Soc.* **52** (1969) 443.
26. ASTM C373-72, "Water Absorption, Bulk Density, Apparent Porosity and Apparent Specific Gravity of Fired Whiteware Products" (ASTM, Philadelphia, 1972).
27. E. M. LEVIN, C. R. ROBBINS and H. F. McMURDIE, "Phase Diagrams for Ceramists" (American Ceramic Society, Westerville, Ohio, 1964) Figs 297, 298 and 1969 Supplement Fig. 2334.
28. U. BALACHANDRAN and N. G. EROR, *J. Electrochem. Soc.* **129** (1982) 1021.
29. S. N. RUDDLESDEN and P. POPPER, *Acta. Crystallogr.* **11** (1958) 54.
30. K. R. UDAYAKUMAR and A. N. CORMACK, *J. Phys. Chem. Solids.* **50** (1989) 55.
31. A. E. PALADINO, *J. Amer. Ceram. Soc.* **48** (1965) 476.
32. S. G. CHO and P. F. JOHNSON, *Ferroelectrics* **132** (1992) 115.

Received 21 January
and accepted 8 October 1993